Structural and magnetic instabilities in ultrathin Fe-rich alloy films on Cu(100)

R. Thamankar, S. Bhagwat, and F. O. Schumann
Freie Universität Berlin, Institut für Experimentalphysik, Arnimallee 14, 14195 Berlin, Germany
(Received 22 April 2003; revised manuscript received 25 September 2003; published 23 February 2004)

A well-known property of Fe/Cu(100) films is the existence of ''magnetic live surface layers'' above ~4 ML (monolayer). This is correlated with structural changes as seen with low electron energy diffraction. Up to ~4 ML a $(n\times1)$ diffraction pattern is observed with $n\sim5$. This changes into a pattern with a (2×1) symmetry for thicker films. We have studied the evolution of the structural and magnetic properties of Fe_xNi_{1-x} and Fe_xMn_{1-x}/Cu(100) films with Fe contents above 80%. The magnetic studies indicate two types of magnetic behavior. Initially the films are uniformly magnetized as judged from the thickness dependence of the Kerr signal. In this thickness regime the $(n\times1)$ diffraction pattern shows a thickness dependence of *n*. For all samples we find that *n* varies linearly from 4–6 in the thickness regime 2–4 ML. The uniformly magnetized state is followed by a phase with constant Kerr intensity. This change in the magnetic properties is accompanied by a change in the diffraction pattern which becomes either (2×1) or $p(1\times1)$. Further, we find the easy axis is normal to the surface for the uniformly magnetized films and magnetic live surface layers. We discuss our results in the context of a nanomartensitic bcc phase recently observed for Fe/Cu(100).

DOI: 10.1103/PhysRevB.69.054419 PACS number(s): 75.70.Ak, 75.50.Bb, 75.70.Rf

I. INTRODUCTION

Ultrathin Fe/Cu(100) films have been extensively investigated in the recent decade.[1–17] A driving force behind this effort was the prediction of a magnetic instability of the fcc phase close to the lattice constant of Cu.[18] Experimentally the following facts are well established for room-temperature grown films. First for thicknesses below ~5 ML (monolayer) the whole films contribute to the magnetic signal, with an out-of-plane orientation of the magnetization *M*. Above this thickness only the first two top layers contribute to the magnetic signal, which is still out of plane.[10] The rest of the film is in a paramagnetic or antiferromagnetic state.[10,15] This unusual feature has been termed ''magnetic live surface layers.''[10] Although it is the disappearance of the magnetism in the interior layers which takes place. In the following we want to abbreviate this feature with SL. This transition in magnetic properties is accompanied by structural changes. Ultrathin Fe/Cu(100) films exhibit complex structures, which are manifested in reconstructions of the low electron energy diffraction (LEED) pattern.[5,14,19] In particular the SL are tied to the appearance of a (2×1) LEED pattern.[14,10] The uniformly magnetized state is accompanied by a (4×1) or (5×1) reconstruction depending on the thickness.[10,20] This structural instability could be related to the well-known atomic volume–magnetic moment instability of bulk fcc Fe predicted previously.[18] Therefore it was concluded that ferromagnetic layers are on top of an antiferromagnetic phase.[14,10] Experimentally one finds an atomic volume of 11.4 $Å^3$ and 12.1 $Å^3$ for the antiferromagnetic and ferromagnetic phase, respectively. It is appealing to calculate the lattice constants of a cubic structure having the same atomic volumes. Using the Cu lattice constant as a reference one finds that only an ~1% reduction (expansion) results in an antiferromagnetic (ferromagnetic) structure.

This picture has been recently challenged as far as the source of the ferromagnetism is concerned.[21,22] A bcc(110) face can never achieve a perfect match on an underlining fcc(100) substrate. However, Biedermann *et al.* find that a tensile strain along the bcc[112] direction results in a commensurate alignment of bcc[111] rows with the fcc(100) surface. The resulting strain energy is compensated by the gain in magnetic energy. From their scanning tunnel microscope (STM) work Biedermann *et al.* suggest that a distorted bcc or nanomartensitic bcc phase carries the ferromagnetism. The fcc phase is supposed to display antiferromagnetic order in agreement with previous work. This observation has been supported by theoretical investigations, which showed that fcc Fe/Cu(100) displays a surprising shear instability.[23] The resulting structure was identified as a bcc derived phase, since the density of states displays the characteristic bcc bonding-antibonding features.[23] Furthermore, Biedermann *et al.* suggest that alloying changes the subtle energy balance significantly hence affecting this structural transition. We have recently demonstrated that starting at ~ 80% Fe content Fe_xNi_{1-x} films show also SL.[24] This we could correlate with structural changes as seen in the LEED pattern. In the light of the recent results by Biedermann *et al.* we present a more detailed structural analysis for Fe_xNi_{1-x}/Cu(100) films. Additionally we extended the studies to Fe_xMn_{1-x}/Cu(100) alloy films. These two alloy systems are particularly suited, because of their properties in the bulk. In Fig. 1 we show a simplified phase diagram where the concentration dependence of the critical temperatures is plotted. The focus is on ferromagnetism in the bcc phase and antiferromagnetism in the fcc phase. Like bulk Fe both systems are stable in the bcc phase at room temperature if the Fe content is above ~80% for Fe_xNi_{1-x} (90% for Fe_xMn_{1-x}).[25,26] In the bulk Fe_xMn_{1-x} alloys are stable in the fcc phase if the Fe content lies between 80% and 50%. In this regime one observes a monotonic increase of the Néel temperature T_N upon increase of the Mn content. At 80% Fe T_N has a value of ~360 K compared to ~500 K for 50% Fe. For Fe contents above 90% Fe_xMn_{1-x} is in bcc phase, which displays ferromagnetic behavior. The Curie temperature T_C decreases linearly in this regime and at 90% Fe T_C is around 500 K

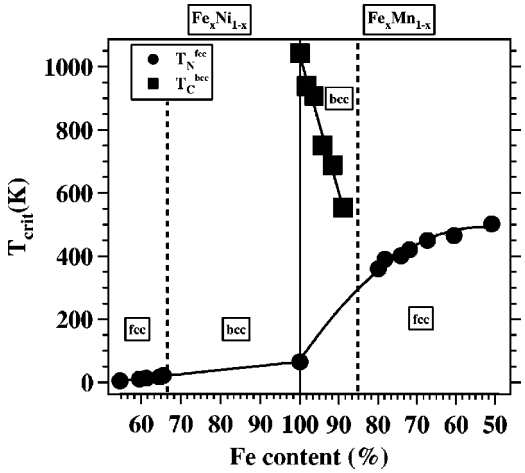

FIG. 1. Simplified phase diagram and critical temperatures for bulk Fe_xNi_{1-x} and Fe_xMn_{1-x} alloys. (Refs. 25–27) The vertical line separates Fe_xNi_{1-x} (left half) and Fe_xMn_{1-x} (right half). The dashed lines divide the fcc from the bcc phase. The solid lines through the T_{crit} data serve as a guide for the eye.

which is ~50% of the value of bcc Fe.[26] Bulk Fe_xNi_{1-x} also shows a complex magnetic behavior. Ferromagnetism in the fcc phase is observed for Fe contents up to ~65%. At this concentration this alloy system displays the well-known anomalies related to the invar effect.[25] In the vicinity of the invar transition there is a coexistence between ferromagnetism and antiferromagnetism.[27] In the regime of bcc stability T_C cannot be determined because before the critical point is reached a transition to a fcc structure is observed. The T_N value for fcc Fe stems from measurements of fcc Fe precipitates in a Cu matrix.[28] We want to address the following questions.

(1) What is the structure of Fe-rich Fe_xNi_{1-x} and Fe_xMn_{1-x} alloys? In particular do they display a similar sequence of LEED reconstructions such as Fe/Cu(100)? This would point towards a bcc derived phase following the work of Biedermann and co-workers[21,22]

(2) If LEED reconstructions such as Fe/Cu(100) exist, how much Fe can be replaced till these reconstructions disappear? Biedermann *et al.* suggest that a subtle energy balance exists, which might be affected by alloying.[21,22]

(3) It was previously accepted that fcc Fe on Cu(100) can be stabilized. Now it appears that a bcc phase evolves. Rather than expecting fcc stable alloy films on Cu(100) we may extend the regime of bcc stability compared to the bulk. We are particularly interested in Fe_xMn_{1-x} alloys due to the complex magnetic properties of Mn. Extending the bcc phase has been demonstrated for thick Fe_xMn_{1-x}/GaAs(001) films.[29]

(4) In this case one would like to know what the magnetic properties in the extended regime are. Further, is there a correlation between structure and the occurrence of SL?

We will show that alloying with up to 20% Ni or Mn maintains the sequence of LEED reconstructions known from Fe/Cu(100). From this we conclude that a distorted bcc phase is present in this concentration regime. In this sense we have extended the bcc phase stability of Fe_xMn_{1-x} alloys when compared with the bulk. The films show an out-of-plane magnetization M in the uniformly magnetized state. Further we find that the emergence of SL at about 4 ML is tied to structural changes yet maintaining a perpendicular orientation of M.

II. EXPERIMENT

The experiments were performed in an UHV chamber (1×10^{-10} mbar) equipped with a LEED optics for structural analysis and CMA (cylindrical mirror analyzer) for chemical analysis. A second electron gun for reflection high-energy electron diffraction (RHEED) studies during the growth is available. E-beam sources were used for the deposition of Fe, Ni, and Mn. All films investigated in this work were grown at room temperature. The rate of all evaporators can be controlled by individual quartz crystal monitors. In order to calibrate these thickness monitors we used RHEED oscillations, which are well documented for Ni/Cu(100) and Fe/Cu(100). The calibration of the Mn evaporator is not so straightforward since no RHEED oscillations for Mn/Cu(100) exist. We adopted the following procedure for calibration of the Mn source. Similar to the recent observations of Offi *et al.* we can observe RHEED oscillations for an ~$Fe_{50}Mn_{50}$ alloy during the growth on Cu(100).[30] From this experiment we can determine the total thickness of the alloy film. Since the Fe source is already calibrated we know the amount of Fe deposited. From the difference of the total thickness and the Fe contribution we can calculate the Mn contribution. This gives us the calibration value for the Mn source. Additionally we use Auger spectroscopy to determine the Fe concentration. Since we know the Fe amount we can determine the Mn contribution to yield the concentration measured with Auger spectroscopy. Again we have a way to calibrate the Mn source, confirming the result from the RHEED experiment. In regular intervals the calibration values were checked, which we found to be stable within 5%. A well-ordered Cu(100) surface was prepared by using Ar^+ sputtering and annealing to 720 K. Alloy films were deposited at 300 K by simultaneous deposition. At present the lowest temperature we can achieve is 110 K with LN_2 cooling. For magnetic measurements we utilized the magneto-optical Kerr effect; our setup allows us to perform these experiments at the growth position. The in-plane and out-of-plane magnetization can be probed by orthogonal magnets. Therefore no sample movement is necessary for Kerr measurements along the in-plane and out-of-plane direction. The maximum available field is at present ~1000 G.

We continue by addressing segregation and clustering effects in alloy thin films. For Fe_xNi_{1-x} alloys Ni surface segregation was observed previously with an enhancement of ~4–7 %.[31–33] Although these investigations continued only up to ~70 % Fe it appears reasonable to assume a small Ni segregation also for Fe-rich alloys. For Fe_xMn_{1-x} alloys we are not aware of similar studies hence we used Auger spectroscopy with low (47 and 40 eV) and high kinetic-energy Auger peaks (703 and 542 eV) of Fe and Mn, respectively. The angle of the incident electron beam was 55° with respect to the surface normal. For Fe-rich alloys the observation of

the Mn 40 eV peak is not possible due to the strong Fe 47 eV peak which extends into the Mn 40 eV peak. However, we find clear evidence of Fe segregation for 50–70 % Fe which amounts to an enhancement of $\sim 10\,\%$.[34] For Fe-rich Fe_xMn_{1-x} alloys we also expect some Fe segregation to occur. We conclude that in both alloy systems the top layers have a slightly different content compared to the volume of the film. Due to the small effect we will neglect this in the following. The lattice mismatch between film and substrate results in a buildup of strain energy in the film. It is now well established that strain can promote alloying of bulk immiscible metals.[35] To our knowledge strain induced dealloying has not been observed for metals. This is in contrast to semiconducting alloys where a composition modulation both lateral and along the growth direction is known to occur though no complete phase separation was detected.[36,37] A theoretical study dealing with the energetics of impurities in Fe finds that Mn and Ni impurities repel each other.[38] We conclude that there is the possibility of some composition variation, but a complete dealloying into Fe and Ni or Mn phases is not likely. Therefore our studies to be presented below reflect the properties of alloys.

III. MAGNETIC LIVE SURFACE LAYERS IN Fe_xNi_{1-x}/Cu(100) FILMS

In Fig. 2(a) we display selected polar hysteresis loops for a $Fe_{92}Ni_8$/Cu(100) sample at different coverages. All loops are square indicating single domain behavior. In the following we do not have to differentiate between remanence and saturation. Further we have normalized the Kerr signals of these loops. In this way we can directly compare the signal levels in Fig. 2(a). If we compare the loop of the 2.1 ML film with the one obtained at 3.2 ML we see a clear increase in the signal level. At 6.4 ML the signal has dropped significantly and is even lower than that for 2.1 ML. Although for a 7.5 ML film the Kerr intensity increases it is still below the level of the 2.1 ML film. We also note that the coercive field H_c has increased considerably.

This variation is very similar to published data for Fe/Cu(100).[39,40] A summary of the magnetic measurements for this alloy is depicted in Fig. 2(b). We observe that the polar Kerr signal increases linearly with thickness for coverages below ~ 4 ML. The dashed line in Fig. 2(b) is a linear fit to the data in this thickness regime. Besides the linear increase we note that the intercept with x axis is near the origin. Both points prove that the film up to ~ 4 ML is uniformly magnetized. Upon further increase of the thickness the polar Kerr signal decreases sharply and is essentially independent of thickness. Although it should be pointed out that previous experiments showed an oscillation of the Kerr intensity.[40,41] If they are present in our case our mesh of data points is too coarse to resolve them. However the important observation is the strong decrease of the Kerr intensity. We find that the signal level is about a quarter of the maximum signal obtained for ~ 4 ML. In other words the observed Kerr signal for thicknesses above 4 ML is equivalent of 1 ML in the uniformly magnetized phase. We conclude that we have observed SL in a $Fe_{92}Ni_8$/Cu(100) sample identical

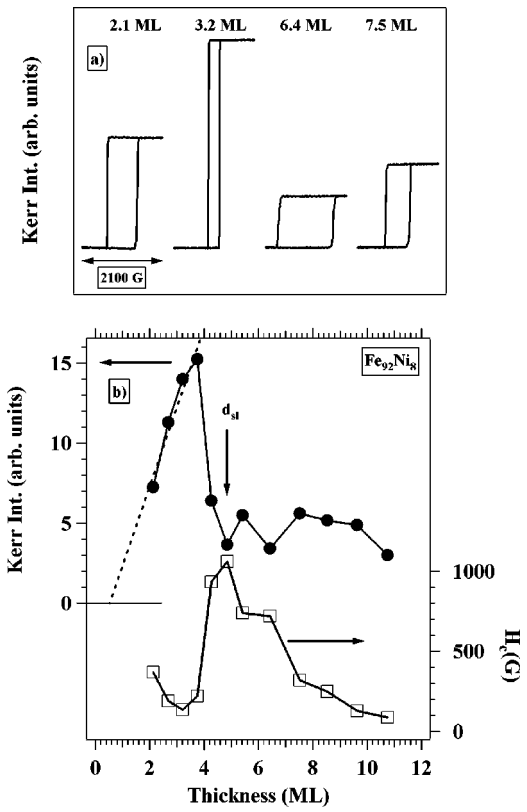

FIG. 2. In panel (a) we show polar hysteresis loops for a $Fe_{92}Ni_8$/Cu(100) alloy at 110 K. The thickness dependence of the remanent Kerr intensity (●) and coercive field (□) is shown in panel (b). The dashed line represents a linear fit to the intensity data.

to the observation of Thomassen *et al.* for Fe/Cu(100).[10] The onset of this behavior has been characterized by the thickness d_{sl}, see Fig. 2(b). Similar experiments have been performed for other concentrations and the variation of d_{sl} on the Fe content was determined.[24] The changes in magnetic behavior are correlated by changes in the structure as we will show now. We have recently demonstrated that SL emerge when a (5×1) reconstruction in the LEED pattern has transformed into a (2×1) or (1×1) structure.[24] In the next section we want to give a more detailed account of this behavior.

IV. STRUCTURE OF FE-RICH Fe_xNi_{1-x} FILMS AND Fe_xMn_{1-x} FILMS

In Fig. 3 we show representative LEED images for a Fe, $Fe_{89}Ni_{11}$, and a $Fe_{90}Mn_{10}$ sample collected at 110 K. On the left half we see the images taken at coverages just below the thickness d_{sl}; in other words uniformly magnetized specimens are given. For all samples a clear $(n\times1)$ reconstruction was detectable. A first look yields a value $n\sim5$. The right half of Fig. 3 shows images taken at coverages above d_{sl}. It is immediately clear that the symmetry of the pattern has changed. In the case of Fe and $Fe_{90}Mn_{10}$ we observe a weak (2×1) pattern whereas the $Fe_{89}Ni_{11}$ alloy displays a (1×1) pattern. Recalling the magnetic measurements shown

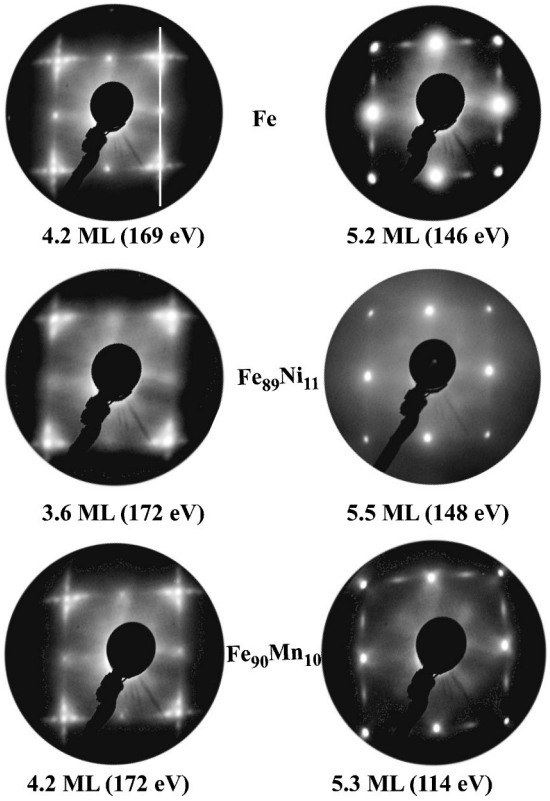

FIG. 3. LEED images for Fe, $Fe_{89}Ni_{11}$, and $Fe_{90}Mn_{10}$ on Cu(100) obtained at 110 K. On the left half a $\sim(5\times1)$ reconstruction can be observed. On the right one sees changes due to a thickness increase. For Fe and $Fe_{90}Mn_{10}$ we observe a (2×1) structure. For $Fe_{89}Ni_{11}$ no reconstruction can be seen. In the pattern of 4.2 ML Fe we have indicated how linescans are being performed.

in Fig. 2 it becomes apparent that there is a correlation between the occurrence of SL and structural changes as presented recently.[24] In this section we want to go beyond the analysis presented in our previous work. The LEED images obtained can be quantitatively analyzed in the following fashion. We performed linescans by going from the (11) to the $(1\bar{1})$ diffraction spots and equivalent pairs as indicated in Fig. 3. The beam energy was $\sim$170 eV. The resulting profile is shown in Fig. 4 for a $Fe_{94}Ni_6$, Fe, and $Fe_{90}Mn_{10}$ sample. The extra intensity due to the reconstructions is easily visible and the associated peaks have been highlighted by gray shading. The three vertical lines indicate the position of the integer peaks. We start the discussion with the well-documented Fe/Cu(100) case. At 2.5 ML the extra intensity is relatively low. Upon increasing the thickness we observe an intensity increase of these spots. This is accompanied by a shift towards the main diffraction spots. This shift is indicated by the dashed lines. At 6.2 ML the extraspots have disappeared and a (2×1) reconstruction is visible, see Fig. 3. Although this is best observed at $\sim$146 eV. The extraspots of the (2×1) reconstruction are marked by the arrows in Fig. 4. Further we notice that the diffraction peaks have become sharper. This indicates that the $\sim(5\times1)$ reconstruction has really disappeared rather than masked by the main peaks. We continue with the discussion of the $Fe_{94}Ni_6$ sample. Again the extra intensity moves towards the main peak as the thickness is increased. At a coverage of 4.2 ML the extraspots have disappeared. At this point the peaks become sharper similar to the Fe/Cu(100) case. The difference we note is that the extra intensity decreases as the thickness is increased. We now move on to the $Fe_{90}Mn_{10}$ alloy. At 1.9 ML we can clearly identify extraspots. For 3.0 ML we observe that the relative intensity of these spots has increased. Again these

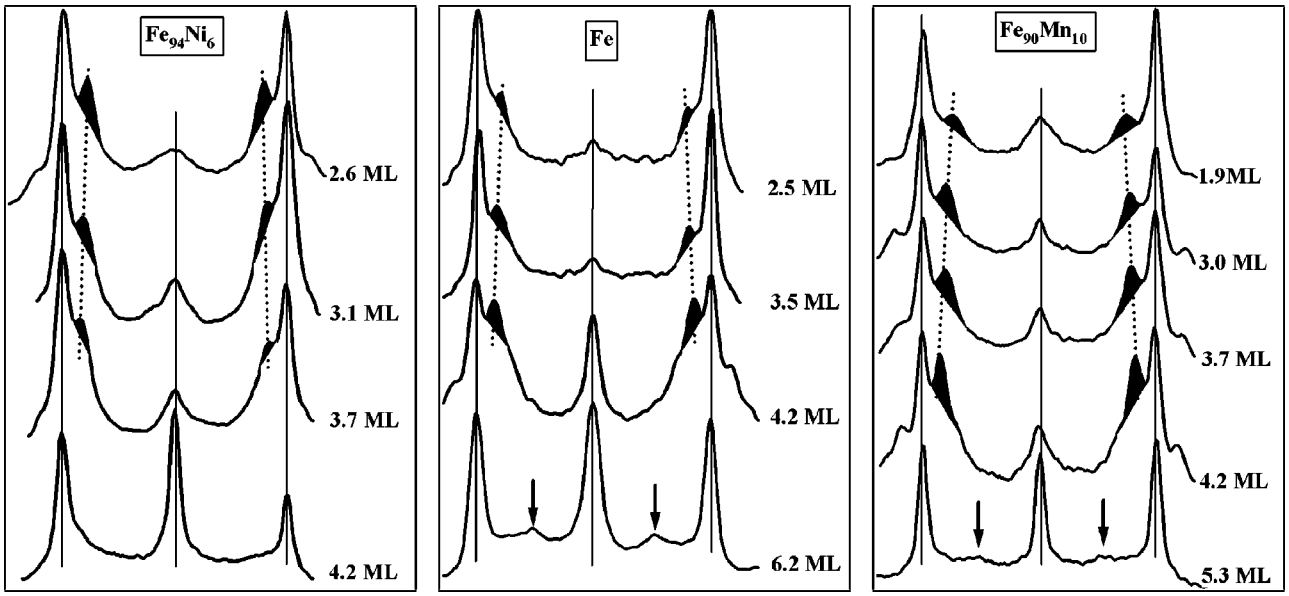

FIG. 4. Linescans through LEED images for a $Fe_{94}Ni_6$, Fe and $Fe_{90}Mn_{10}$ sample at various thicknesses. The measuring temperature was 110 K. The vertical lines indicate the positions of the LEED spots associated to the unreconstructed case. The gray peaks are due to the $(n\times1)$ reconstruction. The vertical dashed lines show that the positions of the extraspots is thickness dependent. Arrows in the plots for Fe and $Fe_{90}Mn_{10}$ indicate a (2×1) reconstruction at 6.2 and 5.3 ML, respectively.

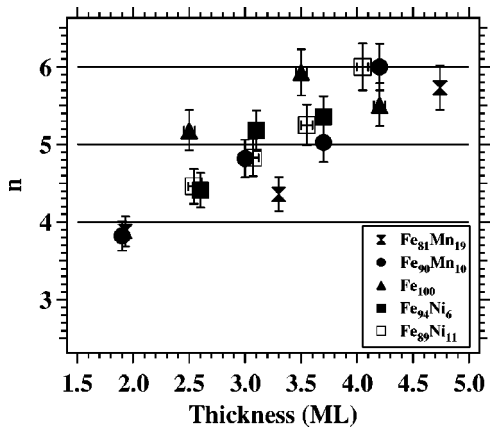

FIG. 5. Thickness dependence of the parameter *n*. The three horizontal lines refer to the integer values 4, 5, and 6.

peaks move towards the nearest integer peak. This trend is continued up to 4.2 ML where the extraspots are best resolved. At 5.3 ML the LEED image has changed to a (2×1) pattern. Weak extraspots halfway in between the integer spots indicate the presence of a (2×1) reconstruction. We conclude that the structural properties of Fe_xNi_{1-x}, Fe and $Fe_{90}Mn_{10}$ samples are identical. These kinds of observations we could make until the Fe content was ~80% for both alloy systems. For Fe_xMn_{1-x} alloys we noted an abrupt change in the structural properties if the Fe content was below 80%. Rather than a thickness dependent $(n\times1)$ reconstruction we saw a $p(1\times1)$ with a weak $c(2\times2)$ structure. At the same time we were not able to detect any ferromagnetic signal. According to the bulk phase diagram we have reached the antiferromagnetic fcc phase. We have determined the position of the extra spots in two ways. First we determine the position by looking at the maximum intensity of the extraspots. Second we employed a linefit. In both cases we find virtual identical values. Now we are able to calculate the separation in *k* space of extraspot and mainspot and can determine the parameter *n* of the $(n\times1)$ reconstruction. The result is plotted in Fig. 5 and it becomes apparent that the value of *n* varies between 4 and 6 for all alloys.

We conclude that for Fe contents up to 80% in Fe_xNi_{1-x} and Fe_xMn_{1-x} alloys on Cu(100) the same thickness dependence of the $(n\times1)$ reconstruction is present, see Fig. 5. This behavior suggests that a distorted bcc phase has formed as for Fe/Cu(100).[21,22]

V. MAGNETIC PROPERTIES OF Fe_xMn_{1-x} FILMS

We turn now our attention to the magnetic properties of Fe_xMn_{1-x}/Cu(100) films. Above we have shown that there is a link between the onset of SL and changes in the LEED pattern for Fe_xNi_{1-x}. From the similar structural behavior of Fe-rich Fe_xNi_{1-x} and Fe_xMn_{1-x} alloys we expect also a magnetic instability for Fe_xMn_{1-x} alloy films. Experimental evidence of this conjecture is shown in Fig. 6(a). There we show selected hysteresis loops of a $Fe_{86}Mn_{14}$ sample measured in the polar geometry at 110 K. Again we have plotted the *M-H* loops with a normalized intensity therefore the

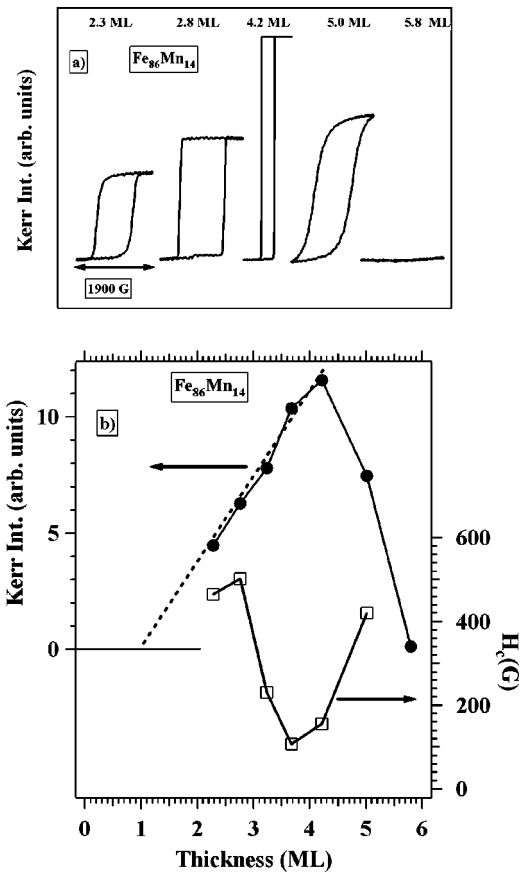

FIG. 6. In panel (a) we show polar loops for a $Fe_{86}Mn_{14}$/Cu(100) sample at 110 K. In panel (b) we plot the polar remanence (●), the dashed line is the result of a linear fit. The thickness dependence of the H_c (□) is shown, too.

height of the loops can be directly compared. Initially we observe a steady increase of the signal, which decreases at 5 ML and vanishes at 5.8 ML. No signal in either field direction could be detected for thickness up to 7.5 ML. In Fig. 6(b) we show the thickness dependence of the out-of-plane remanence and coercive field. A linear fit of the intensity in the interval 2.3–4.2 ML represents a good description. The intercept of this line with the *x* axis occurs slightly below 1 ML. The linear behavior is followed by a sharp decrease of the Kerr signal, which vanishes at 5.8 ML concurrently the coercive field increases. Bulk fcc Fe_xMn_{1-x} alloys with 50–80 % Fe display antiferromagnetic order. From our LEED experiments we know that above ~4 ML a (2×1) or (1×1) structure has evolved. There is consensus that Fe/Cu(100) at this thickness and this LEED pattern is magnetically nonuniform. The top of the film is in a ferromagnetic state, but the interior is in an antiferromagnetic state.[10,12,15,41] It is therefore reasonable to assume that we also observe a fcc structure in the interior. In this case we have to consider the antiferromagnetism of these films, although the concentration is outside the fcc stability in the bulk. Therefore one may ask what causes the lack of a ferromagnetic signal. Two possibilities arise: (i) a rapid increase of H_c quickly exceeding the available field or (ii) a nonmagnetic or antiferromagnetic phase exists. For the first possibility we refer to the

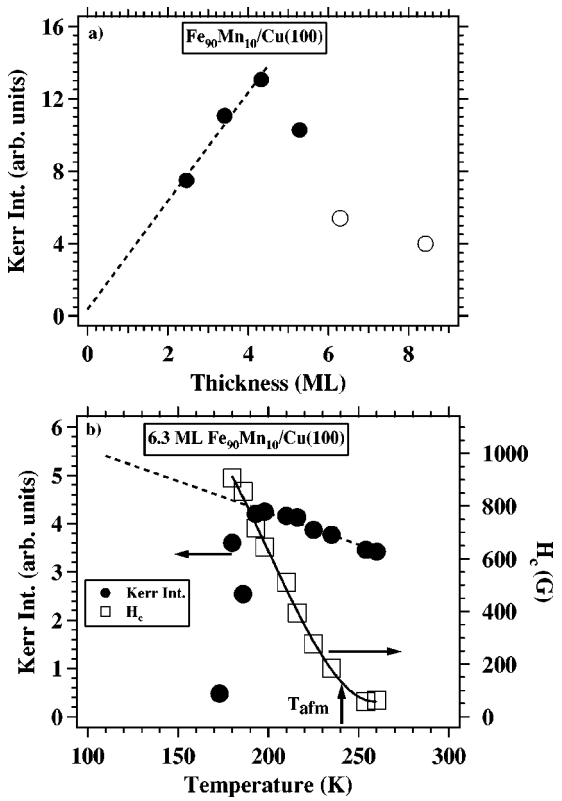

FIG. 7. In panel (a) we show the thickness dependence of the polar remanence for an $Fe_{90}Mn_{10}$ alloy at 110 K. The dashed line represents a linear fit. The open symbols indicate that they have been derived from an extrapolation. In panel (b) we plot the temperature dependence of the polar remanence (left axis) and H_c (right axis) of a 6.3 ML thick film. The linear temperature dependence of the remanence (dashed line) can be used to extrapolate the value at 110 K, which then can be included in panel (a).

work of Qian *et al.*, who report a rapid increase of H_c for Fe/Cu(100) as the temperature is decreased.[40] In order to distinguish between the possibilities we have performed temperature-dependent measurements on a $Fe_{90}Mn_{10}$ sample with identical structural properties. In Fig. 7(a) we see that at 110 K the Kerr intensity rises linearly for thicknesses up to ~4 ML. The dashed line represents a linear fit that intercepts the *x* axis near the origin. This shows that the whole film is magnetic like the previously discussed sample. Above 4 ML we note that the Kerr intensity drops and finally levels out at ~8 ML. There the signal level is ~1.5 ML of the uniformly magnetized state and we conclude that we have SL. The data points denoted by open symbols in Fig. 7(a) have not been collected at 110 K. In agreement with the data shown in Fig. 6 we are not able to detect a signal at 110 K. In order to determine the Kerr signal at 110 K we resorted to an extrapolation. In Fig. 7(b) we show the temperature dependence of the polar remanence and the coercive field for 6.3 ML $Fe_{90}Mn_{10}$. It is apparent that for temperatures below ~200 K no Kerr signal can be detected in agreement with the data displayed in Fig. 6. The reason becomes clear if we consider the behavior of H_c. Although the Kerr signal varies very little in the interval 200–250 K, H_c increases rapidly (by a factor of ~15), exceeding our available fields rapidly.

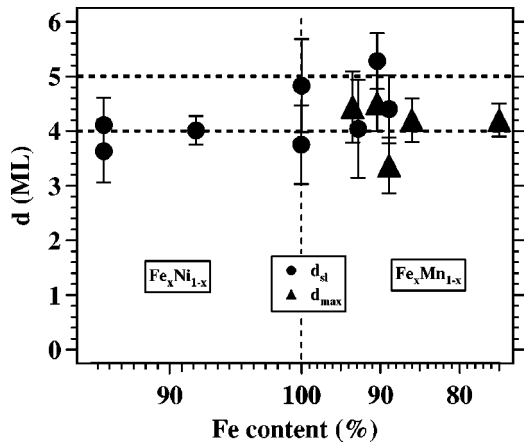

FIG. 8. Concentration dependence of d_{sl} for Fe_xNi_{1-x} (left half) and Fe_xMn_{1-x} (right half). We also plotted d_{max} for Fe_xMn_{1-x}.

From the $H_c(T)$ curve in Fig. 7(b) we can identify a characteristic temperature T_{afm}.[30] It was suggested by Offi *et al.* that this temperature is a measure of T_N of the antiferromagnetic part of the sample. This they concluded from their work on $Fe_{50}Mn_{50}$/Co/Cu(100) films.

The dashed line in Fig. 7(b) is a linear fit to the remanence data. With this curve we extrapolate the Kerr signal at 110 K and plot this in Fig. 7(a). A similar procedure has been adopted for the 8.2 ML film. Like the Fe/Cu(100) and Fe_xNi_{1-x}/Cu(100) case we have SL. Similar observations have been made for all Fe_xMn_{1-x} alloys up to ~80%. In the early stages of the experiments temperature-dependent measurements have not been performed. Therefore we could not determine the thickness d_{sl} for these samples. However the preceding paragraph shows that the thickness where the ferromagnetic signal vanishes (which we call d_{max}) is identical to d_{sl}. Therefore we plot d_{sl} and d_{max} values together in Fig. 8. We can see that SL appear at ~4–5 ML in Fe_xNi_{1-x} and Fe_xMn_{1-x}. The dashed horizontal lines indicate the thickness interval where the $(n\times1)$ reconstruction transforms into a (2×1) or (1×1) pattern. For a $Fe_{92}Mn_8$ sample we also determined the T_C of the ferromagnetic top layer. There we found that the value varied from ~280 K to ~230 K when going from 4 to 8.6 ML. These values are slightly below the ones reported by Thomassen *et al.*[10] but otherwise show the same trend as a function of thickness. From the Kerr signal we judge that ~1.5 ML form the ferromagnetic portion of the SL. Another interesting aspect is the values of the Curie temperatures in the uniformly magnetized state. Work is in progress to determine $T_C(d)$ systematically. However we have some results which tell us when $T_C(d)$ exceeds 300 K. The important observation is that 2.2 ML $Fe_{80}Mn_{20}$ have a $T_C>300$ K. Elmers *et al.* studied bcc Fe(110)/W(110) and found $T_C(2\text{ ML})=480$ K.[42] This is about 46% of the bulk value. If we scale our result on 2.2 ML $Fe_{80}Mn_{20}$ to infinity we would obtain a value of ~650 K. We show in Fig. 1 a rapid decrease of T_C of bulk bcc Fe_xMn_{1-x} upon alloying with Mn. In particular $Fe_{90}Mn_{10}$ has a T_C of ~550 K. It is of course reasonable to assume that the bulk T_C would decrease further for higher Mn contents if the bcc phase would be stable. Therefore our extrapolated value for

''bulk'' $Fe_{80}Mn_{20}$ is surprisingly high if the distorted bcc phase is compared with bcc. Further Biedermann *et al.* state that 3 ML Fe/Cu(100) are not fully bcc, but coexist with antiferromagnetic fcc Fe.[21] They specify that the bcc content increases as a function of thickness and is more than 50% at 3 ML. Clearly this value is smaller for 2 ML thick films.

Another common feature is the orientation of the easy axis. In the uniformly magnetized state and in the regime of SL we find an out-of-plane orientation of M. The uniformly magnetized state extends up to ~ 4 ML, hence a reorientation of M has to be above ~ 4 ML. From our work on $Fe_xNi_{1-x}/Cu(100)$ we found that a positive surface anisotropy K_S caused the perpendicular easy axis in the fcc stability range.[24] For Fe/Cu(100) investigations showed that a positive K_S and volume anisotropy K_V drive M out of plane.[17] These results we compare with properties of bcc(110) Fe films on Ag(111), W(110), and Au(111).[42–44] The first two systems have an in-plane easy axis, but Fe/Au(111) displays an out-of-plane M up to ~ 4 ML. In this case a strong K_S is responsible for a perpendicular M, the K_V term is negligible.[44] Following Biedermann *et al.* we observe a distorted bcc(110) structure, the deviation from cubic symmetry can result in important contributions to K_V as observed in Fe/Cu(100).[17] It would be interesting to determine the individual anisotropy contributions, in particular the volume terms.

VI. SUMMARY

Fe_xNi_{1-x} and Fe_xMn_{1-x} alloys behave very similar as far as structure and magnetism are concerned if the Fe content is above 80%. We summarize as follows.

(i) In both cases we observe $(n\times 1)$ reconstructions in the LEED pattern with $n\sim 4-6$. The thickness dependence of the parameter n does follow a single curve as depicted in Fig. 5. These results are in a agreement with the STM experiments of Biedermann and co-workers.[21,22] Although we are not able to determine the local structure with STM it appears reasonable that the distorted bcc structure observed by Biedermann *et al.* is also present in our samples.

(ii) The regime over which the $(n\times 1)$ structure exists is rather extended. This can be made clear if we consider the change in electron count. In an $Fe_{80}Ni_{20}$ alloy we have 26.4 electrons/atom compared to 25.8 electrons/atom for an $Fe_{80}Mn_{20}$ alloy. This means that varying the electron count by 0.6 electrons/atom does not affect the appearance of the $(n\times 1)$ reconstruction. We conclude that contrary to the suggestion of Biedermann *et al.* alloying with Ni and Mn has no dramatic effect on the relevant energy balance.

(iii) We are able to observe a distorted bcc phase until 80% Fe. In this sense we have extended the bcc phase when compared with the bulk value of 90% Fe. This would agree well with the observations of Jing *et al.* on $Fe_xMn_{1-x}/GaAs(100)$.[29]

(iv) Common magnetic behavior is manifested in the appearance of SL. This is correlated with the disappearance of the $(n\times 1)$ structure and the appearance of a (1×1) or (2×1) structure. Further we observe that the easy axis of the magnetization is out-of-plane for the uniformly magnetized state and SL.

ACKNOWLEDGMENTS

We thank Dr. J. Lindner for critical proof reading. This work was supported by the DFG, Sfb 290 (TP A11).

[1] A. Clarke, P.J. Rous, M. Arnott, G. Jennings, and R.F. Willis, Surf. Sci. **192**, L843 (1987).
[2] D. Pescia, M. Stampanoni, G.L. Bona, A. Vaterlaus, R.F. Willis, and F. Meier, Phys. Rev. Lett. **58**, 2126 (1987).
[3] W.A.A. Macedo and W. Keune, Phys. Rev. Lett. **61**, 475 (1988).
[4] J.R. Dutcher, B. Heinrich, J.F. Cochran, D.A. Steigerwald, and W.F. Egelhoff, Jr., J. Appl. Phys. **63**, 3464 (1988)
[5] W. Daum, C. Stuhlmann, and H. Ibach, Phys. Rev. Lett. **60**, 2741 (1988).
[6] C. Liu, E.R. Moog, and S.D. Bader, Phys. Rev. Lett. **60**, 2422 (1988).
[7] D.P. Pappas, K.P. Kämper, and H. Hopster, Phys. Rev. Lett. **64**, 3179 (1990).
[8] H. Magnan, D. Chandesris, B. Villette, O. Heckmann, and J. Lecante, Phys. Rev. Lett. **67**, 859 (1991).
[9] J.F. Cochran, J.M. Rudd, M. From, B. Heinrich, W. Bennett, W. Schwarzacher, and W.F. Egelhoff, Phys. Rev. B **45**, 4676 (1992).
[10] J. Thomassen, F. May, B. Feldmann, M. Wuttig, and H. Ibach, Phys. Rev. Lett. **69**, 3831 (1992).
[11] R. Allenspach and A. Bischof, Phys. Rev. Lett. **69**, 3385 (1992).
[12] D.J. Keavney, D.F. Storm, J.W. Freeland, I.L. Grigorov, and J.C. Walker, Phys. Rev. Lett. **74**, 4531 (1995).
[13] A. Kirilyuk, J. Giergiel, J. Shen, and J. Kirschner, Phys. Rev. B **52**, R11 672 (1995).
[14] S. Müller, P. Bayer, C. Reischl, K. Heinz, B. Feldmann, H. Zillgen, and M. Wuttig, Phys. Rev. Lett. **74**, 765 (1995).
[15] R.D. Ellerbrock, A. Fuest, A. Schatz, W. Keune, and R.A. Brand, Phys. Rev. Lett. **74**, 3053 (1995).
[16] M. Zharnikov, A. Dittschar, W. Kuch, C.M. Schneider, and J. Kirschner, Phys. Rev. Lett. **76**, 4620 (1996).
[17] W. Platow, M. Farle, and K. Baberschke, Europhys. Lett. **43**, 713 (1998).
[18] V.L. Moruzzi, P.M. Marcus, and J. Kübler, Phys. Rev. B **39**, 6957 (1989).
[19] P. Bayer, S. Müller, P. Schmailzl, and K. Heinz, Phys. Rev. B **48**, 17 611 (1993).
[20] K. Heinz, S. Müller, and L. Hammer, J. Phys.: Condens. Matter **11**, 9437 (1999).
[21] A. Biedermann, R. Tscheließnig, M. Schmid, and P. Varga, Phys. Rev. Lett. **87**, 086103 (2001).
[22] A. Biedermann, M. Schmid, and P. Varga, Phys. Rev. Lett. **86**, 464 (2001).
[23] D. Spišák and J. Hafner, Phys. Rev. Lett. **88**, 056101 (2002).
[24] R. Thamankar, A. Ostroukhova, and F.O. Schumann, Phys. Rev. B **66**, 134414 (2002).

[25] E. F. Wassermann, in *Invar: Moment-Volume Instabilities In Transition Metals And Alloys*, Ferromagnetic Materials, Vol. 5, edited by K. H. J. Buschow and E. P. Wohlfarth (North-Holland, Amsterdam, 1990), pp. 238–322.
[26] H. Yamauchi, H. Watanabe, Y. Suzuki, and H. Saito, J. Phys. Soc. Jpn. **36**, 971 (1974).
[27] H. Zähres, M. Acet, W. Stamm, and E.F. Wassermann, J. Magn. Magn. Mater. **72**, 80 (1988).
[28] U. Gonser, C.J. Meechan, A.H. Muir, and H. Wiedersich, J. Appl. Phys. **34**, 2373 (1963).
[29] C. Jing, Y.Z. Wu, Z.X. Yang, G.S. Dong, and X.F. Jin, J. Magn. Magn. Mater. **198-199**, 270 (1999).
[30] F. Offi, W. Kuch, and J. Kirschner, Phys. Rev. B **66**, 064419 (2002).
[31] K. Wandelt and G. Ertl, Surf. Sci. **55**, 403 (1976).
[32] F.O. Schumann, S.Z. Wu, G.J. Mankey, and R.F. Willis, Phys. Rev. B **56**, 2668 (1997).
[33] M.G. Martin, F. Foy, F. Chevrier, G. Krill, and M.C. Asensio, Surf. Sci. **433-435**, 88 (1999).
[34] R. Thamankar, S. Bhagwat, and F. O. Schumann (unpublished).
[35] J. Tersoff, Phys. Rev. Lett. **74**, 434 (1995).
[36] S.P. Ahrenkiel, S.H. Xin, P.M. Reimer, J.J. Berry, H. Luo, S. Short, M. Bode, M. Al-Jassim, J.R. Buschert, and J.A. Furdyna, Phys. Rev. Lett. **75**, 1586 (1995).
[37] K.C. Hsieh, J.N. Baillargeon, and K.Y. Cheng, Appl. Phys. Lett. **57**, 2244 (1990).
[38] B. Nonas, K. Wildberger, R. Zeller, and P.H. Dederichs, Phys. Rev. Lett. **80**, 4574 (1998).
[39] A. Berger, B. Feldmann, H. Zillgen, and M. Wuttig, J. Magn. Magn. Mater. **183**, 35 (1998).
[40] D. Qian, X.F. Jin, J. Barthel, M. Klaua, and J. Kirschner, Phys. Rev. Lett. **87**, 227204 (2001).
[41] D. Li, M. Freitag, J. Pearson, Z.Q. Qiu, and S.D. Bader, Phys. Rev. Lett. **72**, 3112 (1994).
[42] H.J. Elmers, J. Hauschild, H. Fritzsche, G. Liu, U. Gradmann, and U. Köhler, Phys. Rev. Lett. **75**, 2031 (1995).
[43] Z.Q. Qiu, J. Pearson, and S.D. Bader, Phys. Rev. Lett. **67**, 1646 (1991).
[44] G. Lugert, W. Robl, L. Pfau, M. Brockmann, and G. Bayreuther, J. Magn. Magn. Mater. **121**, 498 (1993).